

Article

Dynamic Response of Slender Vertical Structures Subjected to Thunderstorm Outflows

Luca Roncallo ^{*}, Matteo Gimondo  and Federica Tubino 

Department of Civil, Chemical and Environmental Engineering (DICCA), Polytechnic School, University of Genoa, Via Montallegro 1, 16145 Genoa, Italy; s4082178@studenti.unige.it (M.G.); federica.tubino@unige.it (F.T.)

* Correspondence: luca.roncallo@edu.unige.it

Abstract: This study examines the maximum alongwind dynamic response of slender vertical structures subjected to thunderstorms, comparing the induced maximum response with the one induced via synoptic events. Two real structures are considered as case studies: a lighting pole and a telecommunications tower. The comparison between thunderstorm- and synoptic-induced dynamic responses is performed through a critical analysis of three ratios characterizing the difference between the two phenomena: the reference wind speed, the mean wind profile, and the gust response factor. The comparison shows that the definition of the reference wind speed and the height of the nose tip of the thunderstorm mean wind profile are crucial for the maximum response, as well as for the dependence of the turbulence intensity on the roughness length. The results show that thunderstorms provide the design loading condition in most cases.

Keywords: thunderstorm outflows; extra-tropical cyclones; gust response factor; vertical slender structures; wind engineering

1. Introduction

Slender vertical structures are sensitive to wind, which usually represents their design loading condition [1] and can induce fatigue-related collapses [2]. While their assessment under stationary wind conditions, such as extra-tropical cyclones, is nowadays consolidated in codes and standards, their reliability under nonstationary conditions caused via thunderstorm outflows is still a matter of research. As shown via meteorological observations [3], experimental measurements in laboratories [4], full-scale analyses of collected wind speed time histories [5], and their comparison with stationary boundary layer winds [6], thunderstorm outflow is characterized via a nose-shaped vertical mean velocity profile and nonstationary turbulent fluctuation. Therefore, most of the models and approaches available for synoptic winds are unsuitable for their representation. In addition, the reference wind velocity provided by codes is currently defined according to statistical analyses that do not distinguish between extra-tropical cyclones and thunderstorms [7]. Indeed, the wind velocities provided by synoptic winds and thunderstorm outflows are characterized by different extreme distributions [8]; in thunderstorm-prone areas, high return period thunderstorm wind speeds can be higher than those corresponding to extra-tropical cyclones, as pointed out by Solari [9] and demonstrated by Zhang et al. [10], who carried out statistical analyses on thunderstorm time histories collected in the High Tyrrhenian Sea. Considering that synoptic winds provide higher wind speeds at greater heights and thunderstorms at lower ones, not only can mid-low structures be under-designed, but taller buildings can be over-designed to wind actions. As a result, since current codes and standards lack a reliable and handy approach for downburst-resistant structural design, the resistance and durability of mid-low structures can be put at risk by the occurrence of such extreme wind conditions, as pointed out by Letchford et al. [11] and investigated by Fu et al. [12], who studied the collapse of transmission towers.



Citation: Roncallo, L.; Gimondo, M.; Tubino, F. Dynamic Response of Slender Vertical Structures Subjected to Thunderstorm Outflows. *Appl. Sci.* **2023**, *13*, 11440. <https://doi.org/10.3390/app132011440>

Academic Editor: Alberto Doria

Received: 27 September 2023

Revised: 10 October 2023

Accepted: 12 October 2023

Published: 18 October 2023



Copyright: © 2023 by the authors. Licensee MDPI, Basel, Switzerland. This article is an open access article distributed under the terms and conditions of the Creative Commons Attribution (CC BY) license (<https://creativecommons.org/licenses/by/4.0/>).

During the last few decades, with the aim of providing engineers with suitable tools to predict the wind loading and maximum structural response to thunderstorms, different approaches were adopted, which can be gathered into two main families: time domain analysis (TDA) and time–frequency domain approaches. Time domain analysis consists of the evaluation of the dynamic response starting from wind velocity time histories that have been recorded full scale [13], simulated in moving jet wind tunnels [14], or simulated numerically starting from suitable statistical models of the wind speed. In particular, Solari et al. [15] proposed a hybrid simulation technique to generate thunderstorm time histories, subsequently adopted by Solari and De Gaetano [16], which consists of the joint usage of Monte Carlo simulations and wind speed data collected at full scale. Although they represent a reliable method, they can be time-consuming, and their use is restricted by the limited set of available full-scale thunderstorm records. Starting from a wide set of thunderstorm records, the thunderstorm response spectrum (TRS) technique was proposed by Solari et al. for single-degree-of-freedom (SDOF) systems [17], which was subsequently extended by Solari for multi-degree-of-freedom (MDOF) systems [18], in analogy to the widely adopted earthquake response spectrum [19]. Despite its simple conceptualization and its reliability being based on a significant amount of data, the usage of the TRS approach lacks handiness due to the absence of analytical formulations and its reliance on charts. Time–frequency domain analysis makes use of advanced models such as the evolutionary power spectral density (EPSD) to account for the nonstationary characteristics of a thunderstorm outflow. In this framework, Roncallo and Solari [20] recently proposed an EPSD model for thunderstorms based on a large number of full-scale records, while Kareem et al. [21] adopted the EPSD to generalize the wind loading chain approach from stationary winds to thunderstorms. Based on such models, the gust factor technique from Davenport [22] was generalized to nonstationary winds by Kwon and Kareem [23], who introduced suitable equivalent parameters, and subsequently, Roncallo et al. [13] removed the hypothesis of long-pulse duration. More recently, closed-form solutions to simplify its application from a design perspective were proposed by Kwon and Kareem [24] under the hypothesis of long-pulse duration. Subsequently, Roncallo and Tubino [25] proposed a new closed-form solution that accounts for the transient dynamic effects of both the nonstationary response and the presence of a background wind. Although this approach is surely convenient and user-friendly, it has the shortcoming of being slightly conservative when the system becomes flexible and low-damped. Moreover, the closed-form solution proposed by Roncallo and Tubino [25], which accounts for the thunderstorm wind speed parameters and the transient effects in the dynamic response, was developed for SDOF systems, and its reliability when applied to MDOF systems needs to be assessed.

In this framework, this study aims to address these shortcomings by pursuing two main objectives: the extension of the Thunderstorm Gust Response Factor (TGRF) technique to the analysis of vertical structures, assessing its reliability, and the comparison between the maximum dynamic response due to thunderstorms and synoptic events. The extension of the TGRF technique to the case of slender vertical structures is pursued by accounting for the variation in the mean wind speed with the height, and for the partial correlation of the turbulent fluctuations along the structure. A suitable model from the literature is introduced to describe the vertical profile of the mean wind speed, while the partial correlation is accounted for through the coherence function from stationary winds, which is suitably adapted to the thunderstorm case as proposed by Solari [18]. Subsequently, the reliability of the TGRF is assessed by comparing the related maximum response with the one estimated via TDA based on a large number of full-scale thunderstorm records, and the TRS technique. Finally, the maximum dynamic response induced via thunderstorms is compared with the one induced by stationary synoptic winds. The comparison between thunderstorm- and synoptic-induced dynamic responses is based on the definition of three factors depending on the reference: wind velocity, the mean wind vertical profile, and the gust response factor. Two structures of different heights and dynamical properties are

considered as case studies: a steel lighting pole, representative of a low-rise structure, and a reinforced concrete telecommunications tower, representative of a taller structure.

The paper is organized as follows: Section 2 outlines the analytical formulation, starting with the extension of the EPSD-based approach to continuous systems and deriving the dynamic response of a slender vertical structure along with its maximum value through the TGRF technique. Section 3 illustrates the numerical applications, including the structure case studies chosen, the wind speed data utilized, the modeling of the wind loading, and the comparison between the estimate of the maximum dynamic response using the TGRF, TDA, and TRS techniques. Section 4 outlines the comparison between the dynamic response induced by synoptic winds and thunderstorm outflows, estimated following a design-based approach and by investigating the role of different assumptions for the turbulence intensity profile. Finally, Section 5 derives the conclusions and prospects of this research. Appendix A reports the models of the vertical profiles of the wind speed and turbulence intensity, and the model for the integral length scale adopted in this study.

2. Analytical Formulation

In this section, the analytical framework describing the wind speed modeling and the dynamic response of mono-dimensional structures to thunderstorm outflow is outlined. Firstly (Section 2.1), the analytical model of the wind speed along a vertical linear domain is presented [18], which extends the single-point EPSD model of thunderstorm winds [20]. Second (Section 2.2), the model is adopted to derive the dynamic response of slender vertical structures, assuming that it is dominated by the first mode of vibration. Then (Section 2.3), the TGRF for the estimate of the maximum dynamic response is described.

2.1. Wind Velocity

Let us consider the horizontal non-directional wind speed of a thunderstorm outflow along a vertical linear domain defined by the spatial coordinate z (with $z = 0$ m at the ground level). The wind speed can be decomposed as follows [18,26–28]:

$$v(z, t) = \bar{v}(z, t) + v'(z, t) \quad (1)$$

where $\bar{v}(z, t)$ and $v'(z, t)$ are the slowly varying mean wind speed and the residual turbulent fluctuations, respectively. They can be expressed as:

$$\bar{v}(z, t) = \bar{v}_{\max}(h)\alpha(z)\gamma(t) \quad (2)$$

$$v'(z, t) = \bar{v}_{\max}(h)\bar{I}_v(h)\alpha(z)\theta(z)\gamma(t)\tilde{v}'(z, t) \quad (3)$$

where $\alpha(z)$ and $\theta(z)$ are the vertical profiles of the mean wind velocity and turbulence intensity (Appendix A), respectively, $\gamma(t)$ is the modulating function of the slowly varying mean speed, $\bar{I}_v(h)$ is the mean value of the turbulence intensity [13,18,20,29] at the reference height h at which the wind velocity is assigned, and $\tilde{v}'(z, t)$ are the reduced turbulent fluctuations, dealt with as a stationary and Gaussian process with zero mean and unitary standard deviation.

It is worth pointing out that in Equations (2) and (3), the vertical profiles of the mean speed and turbulence intensity are assumed to be independent of time [27,30,31]. This is somehow in contrast with the experimental observations, which indicate that both these quantities evolve over time during the development of the downburst [5,32,33], and that in particular, the characteristic nose-shaped profile of the mean speed is clearly noticeable solely during the ramp-up phase of the wind speed. However, since there are no well-established analytical models in the literature that suitably describe their evolution over time, such vertical profiles are assumed as independent of time. The reliability of this assumption for the mean wind speed, widely used in the literature [15,18,24,26,34], is partially justified by the fact that the nose-shaped profile is noticeable within a time interval

in which the mean wind velocity reaches its maximum, and is thus in the neighborhood of the instant when the maximum response is expected [13,32,35].

The residual fluctuations in Equation (3) are a uniformly modulated process and can be characterized through their cross-evolutionary power spectral density (CEPSD):

$$S_{v'v'}(z, z', t, n) = \bar{v}_{\max}^2 \bar{I}_v^2(h) \gamma^2(t) \alpha(z) \alpha(z') \theta(z) \theta(z') S_{\tilde{v}'\tilde{v}'}(z, z', n) \tag{4}$$

where $S_{\tilde{v}'\tilde{v}'}(z, z', n)$ is the cross-power spectral density (CPSD) of the reduced turbulent fluctuations, which can be written as follows:

$$S_{\tilde{v}'\tilde{v}'}(z, z', n) = \sqrt{S_{\tilde{v}'}(z, n) S_{\tilde{v}'}(z', n)} \text{Coh}_{\tilde{v}'\tilde{v}'}(z, z', n) \tag{5}$$

In Equation (5), $\text{Coh}_{\tilde{v}'\tilde{v}'}(z, z', n)$ is the coherence function of the reduced turbulent fluctuations $\tilde{v}'(z, t)$ between two points, z and z' ; it is assumed to be time-invariant. In accordance with [18], the coherence function is defined as:

$$\text{Coh}_{\tilde{v}'\tilde{v}'}(z, z', n) = \exp\left\{ \frac{2nc_z|z - z'|}{\bar{v}_{\max}(z) - \bar{v}_{\max}(z')} \right\} \tag{6}$$

where c_z is the exponential decay coefficient of $\tilde{v}'(z, t)$ along z . It is important to notice that the hypothesis of the time-invariant vertical profile allows us to treat the coherence function between the processes $v'(z, t)$ and $v'(z', t)$ as independent of time, being the modulating function $\gamma(t)$, which is independent of height. An evolutionary model for the coherence function related to non-stationary winds was proposed by [36], who showed how neglecting the time dependence may not be conservative for the estimate of the standard deviation of the dynamic response. However, in this study, the wind speed is assumed to be uniformly modulated, and thus these contributions are neglected, leading to a simplification of the analyses and allowing us to carry out a comparison with other approaches based on the same assumption (i.e., TDA and TRS).

2.2. Dynamic Response

Let us consider a slender vertical structure schematized as a linear elastic continuous system. The alongwind force per unit length due to the wind speed in Equation (1) reads:

$$f(z, t) = \frac{1}{2} \rho v^2(z, t) b(z) c_D(z) \tag{7}$$

where $b(z)$ is the width of the face exposed to the wind. Substituting Equation (1) into Equation (7), the wind loading can be expressed as the sum of a mean and fluctuating part as follows:

$$f(z, t) = \bar{f}(z, t) + f'(z, t) \tag{8}$$

Invoking the hypothesis of small turbulence, the mean, and the fluctuating parts of the loading read, respectively:

$$\bar{f}(z, t) = \frac{1}{2} \rho \bar{v}_{\max}^2(h) \gamma^2(t) \alpha^2(z) b(z) c_D(z) \tag{9}$$

$$f'(z, t) = \rho \bar{v}_{\max}^2(h) \bar{I}_v(h) \gamma^2(t) \alpha^2(z) \theta(z) b(z) c_D(z) \tilde{v}'(z, t) \tag{10}$$

It can be observed in Equation (10) that the fluctuating part of the loading is a uniformly modulated process.

Let us assume that the dynamic response to thunderstorm outflows is dominated by the first mode of vibration; therefore, the alongwind displacement reads:

$$x(z, t) = \psi_1(z) p_1(t) \tag{11}$$

where $\psi_1(z)$ is the first modal shape and $p_1(t)$ is the first principal coordinate, the solution of the equation of motion:

$$\ddot{p}_1(t) + 2\omega_1\zeta\dot{p}_1(t) + \omega_1^2 p_1(t) = \frac{1}{m_1} f_1(t) \tag{12}$$

where $\omega_1 = 2\pi n_1$ is the first circular modal frequency, m_1 is the first modal mass, and $f_1(t)$ is the first modal force defined as:

$$f_1(t) = \int_0^H f(z,t)\psi_1(z)dz \tag{13}$$

where H is the height of the structure. Substituting Equations (8)–(10) in Equation (13), the modal force can also be written as the sum of a mean and fluctuating part:

$$f_1(t) = \bar{f}_1(t) + f'_1(t) \tag{14}$$

where $\bar{f}_1(t)$ and $f'_1(t)$ read:

$$\bar{f}_1(t) = \frac{1}{2}\rho\bar{v}_{\max}^2(h)\gamma^2(t)a_1 \tag{15}$$

$$f'_1(t) = \rho\bar{v}_{\max}^2(h)\bar{I}_v(h)a_1\gamma^2(t)\tilde{a}'_1(t) \tag{16}$$

respectively, where a_1 has the dimension of an area and can be interpreted as the area perceived by the wind on the first mode, while $\tilde{a}'_1(t)$ is a non-dimensional function of time. The two quantities are defined as follows:

$$a_1 = \int_0^H \alpha^2(z)b(z)c_D(z)\psi_1(z)dz \tag{17}$$

$$\tilde{a}'_1(t) = \frac{1}{a_1}\int_0^H \alpha^2(z)\theta(z)b(z)c_D(z)\bar{v}'(z,t)\psi_1(z)dz \tag{18}$$

Substituting Equation (14) in Equation (12), the first principal coordinate can be decomposed as follows:

$$p_1(t) = \bar{p}_1(t) + p'_1(t) \tag{19}$$

where the mean part $\bar{p}_1(t)$ is assumed as the static response to the mean part of the loading $\bar{f}_1(t)$ (Equation (15)):

$$\bar{p}_1(t) = \frac{1}{2m_1(2\pi n_1)^2}\rho\bar{v}_{\max}^2(h)\gamma^2(t)a_1 \tag{20}$$

The fluctuating part $p'_1(t)$ is characterized by its EPSD:

$$S_{p'_1}(n,t) = \left[\rho\bar{v}_{\max}^2(h)\bar{I}_v(h)a_1\right]^2 |Z_1(n,t)|^2 S_{\tilde{a}'_1}(n) \tag{21}$$

where $Z_1(n,t)$ is the evolutionary frequency response function (EFRF) related to the first mode, and $S_{\tilde{a}'_1}(n)$ is the PSD of $\tilde{a}'_1(t)$:

$$Z_1(n,t) = \int_{-\infty}^t h_1(t-\tau)e^{-i2\pi n(t-\tau)}\gamma^2(\tau)d\tau \tag{22}$$

$$S_{\tilde{a}_1}(n) = \frac{1}{a_1^2} \int_0^H \int_0^H \alpha^2(z)\alpha^2(z')\theta(z)\theta(z')b(z)b(z')c_D(z)c_D(z')\psi_1(z)\psi_1(z')S_{\tilde{v}'\tilde{v}'}(z, z', n)dzdz' \tag{23}$$

where $h_1(t)$ is the impulse response function associated with the first mode of vibration. It is worth pointing out that the generalization to MDOF of the EFRF method is pursued here following a mode-by-mode approach (Equation (21)), which offers the advantage of overcoming potential limitations of the EFRF when applied to MDOF systems [37].

2.3. Maximum Dynamic Response: Thunderstorm Gust Response Factor Technique

In this section, the derivation of the maximum dynamic response is outlined by employing the TGRF technique [13,38], benefiting from the closed-form solution proposed by Roncallo and Tubino [25]. The TGRF constitutes a generalization of the gust response factor from Davenport [22] for thunderstorms, accounting for the transient dynamic effects due to the non-stationarity of the loading and the presence of a background wind [13,38]. It is defined as follows:

$$G_{x,T} = 1 + 2g_x(\tilde{v}_x\tilde{T}_{eq})I_v(z_{eq})C\sqrt{B^2 + R^2} \tag{24}$$

where g_x is the Davenport peak factor [39], B and R are the background and resonance factors, respectively, and \tilde{v}_x is the normalized expected frequency. They read as follows [40–42]:

$$B^2 = \frac{1}{1 + 0.9\left[\frac{b+H}{L_v(z_{eq})}\right]^{0.63}} \tag{25}$$

$$R^2 = \frac{\pi}{4\zeta} S_{\tilde{v}'}(z_{eq}, n_1)\chi_H(\eta_H)\chi_b(\eta_b) \tag{26}$$

$$\eta_\varepsilon = \frac{4n_1\varepsilon}{\tilde{v}_{\max}(z_{eq})} \quad \varepsilon = H, b \tag{27}$$

$$\tilde{v}_x = \sqrt{\frac{R^2}{B^2 + R^2}} \tag{28}$$

where $\chi_\varepsilon (\varepsilon = H, b)$ accounts for the partial correlation of the turbulence along H and b in virtue of the equivalent wind spectrum (EWS) technique [40,42], which operates solely on the reduced turbulent fluctuations $z_{eq} = 0.6H$, and L_v is the integral length scale of the reduced turbulence. In Equation (24), C and \tilde{T}_{eq} are equivalent parameters that can be estimated by employing the closed-form solution proposed by [25]:

$$C^2 = \frac{\gamma^{*20}\left(\frac{\tilde{T}_{\max}}{\tilde{T}_{tot}} - 1\right) + \Lambda^5 - \frac{5}{2}\Lambda^4\Phi + \frac{10}{3}\Lambda^3\Phi^2 - \frac{5}{2}\Lambda^2\Phi^3 + \Lambda\Phi^4 - \frac{1}{6}\Phi^5}{\gamma^{*16}\left(\frac{\tilde{T}_{\max}}{\tilde{T}_{tot}} - 1\right) + \Lambda^4 - 2\Lambda^3\Phi + 2\Lambda^2\Phi^2 - \Lambda\Phi^3 + \frac{1}{5}\Phi^4} \tag{29}$$

$$\tilde{T}_{eq} = \frac{\gamma^{*16}\left(\tilde{T}_{\max} - \tilde{T}_{tot}\right) + \tilde{T}_{tot}\left(\Lambda^4 - 2\Lambda^3\Phi + 2\Lambda^2\Phi^2 - \Lambda\Phi^3 + \frac{1}{5}\Phi^4\right)}{[C^2]^4} \tag{30}$$

where γ^* is defined as the ratio between the background mean wind speed and the maximum mean wind velocity of the thunderstorm outflow [20,38], and the parameters \tilde{T}_{\max} , \tilde{T}_{tot} , Λ , and Φ , which are expressed as follows:

$$\tilde{T}_{\max} = T_{\max}n_1 \tag{31}$$

$$\tilde{T}_{tot} = \tilde{T}_1 + \tilde{T}_N \tag{32}$$

$$\Lambda = \gamma^{*4} + \Phi \tag{33}$$

$$\Phi = \beta(1 - \gamma^{*4}) \tag{34}$$

where $T_{\max} = 600$ s, and:

$$\tilde{T}_1 = \frac{\tilde{T}}{2} \tag{35}$$

$$\tilde{T}_N = \begin{cases} \tilde{T}_2, & \tilde{T}_2 \leq \tilde{T}_{\max}/2 \\ \tilde{T}_{\max}/2, & \text{otherwise} \end{cases} \tag{36}$$

$$\tilde{T}_2 = \tilde{T}_1 \left(1 + \frac{1}{2\xi\tilde{T}} \right) \tag{37}$$

$$\beta = \frac{1}{1 + \frac{1}{4\xi\tilde{T}}} \tag{38}$$

$$\tilde{T} = Tn_1 \tag{39}$$

where T represents the duration of the intense phase of the outflow [20,38]. Once the TGRF is calculated, the maximum response is estimated as follows:

$$x_{\max} = \bar{x}_{\max} G_{x,T} \tag{40}$$

where \bar{x}_{\max} is the maximum value of the mean part of the response evaluated at $z = H$ ($\psi_1(H) = 1$), that reads (Equations (11) and (20)):

$$\bar{x}_{\max} = \frac{1}{2m_1(2\pi n_1)^2} \rho \bar{v}_{\max}^2(h) a_1 \tag{41}$$

Finally, it is worth observing that for the stationary case, $\gamma^* \rightarrow 1$; thus, $\tilde{T}_{eq} \rightarrow \tilde{T}_{\max}$ and $C \rightarrow 1$. Therefore, the TGRF in Equation (24) returns to the classical formulation:

$$G_{x,S} = 1 + 2g_x(\tilde{v}_x \tilde{T}_{\max}) I_v(z_{eq}) \sqrt{B^2 + R^2} \tag{42}$$

3. Numerical Application

In this section, the structure case studies are first described, reporting the geometrical and dynamical properties (Section 3.1). Subsequently, the modeling of the wind velocity and the wind loading is outlined (Section 3.2). Finally, the maximum dynamic response of the two structures provided via the thunderstorm is estimated through the TGRF technique and compared with the one obtained via TDA and TRS (Section 3.3).

3.1. Structure Case Studies

Two slender vertical structures are considered: a steel lighting pole (Figure 1a) and a reinforced concrete telecommunications tower [18] (Figure 1b).

The steel lighting pole (Figure 1a) is composed of a shaft, covered at the base with a prismatic hollow element, and a lighting device at the top. The shaft consists of two parts, both with a truncated conical shape and a tubular octagonal section, with a constant thickness of 4 mm. Its height above the ground is 14 m, of which 2.2 m corresponds to the first part, and 11.8 m to the second one. The outer diameters at the base and at the top are 280 and 80 mm, respectively. It reaches a total height of 15.76 m. The top portion, a length of 1.76 m, holding the lighting device, presents a decagonal cross section until a height of 14.33 m, after which it becomes dodecagonal. The lighting device has a mass of 145 kg and

a center of gravity at 14.9 m above the ground. Considering its modest height, it can be regarded as a low-rise structure.

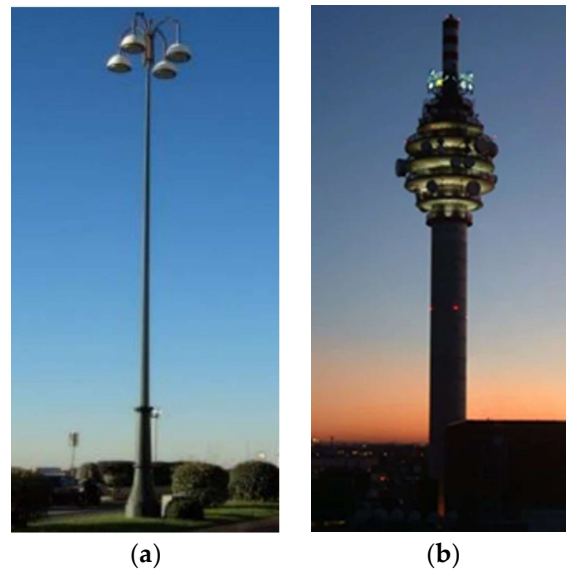


Figure 1. Structure test cases: (a) steel lighting pole; (b) reinforced concrete telecommunications tower.

The reinforced concrete telecommunications tower (Figure 1b) is 98.00 m high and can be regarded as a mid-height structure. It is composed of three superimposed shafts. The first shaft, up to 3.90 m above the ground, is made up of two concentric tubular circular sections linked by six radial walls. The second one, from 3.90 to 80.50 m, has a circular tubular section with an outer diameter of 6.50 m and thickness of 0.50 m; in its upper part, from 59.50 to 80.50 m, there are seven steel platforms with a constant distance of 3.50 m that carry transmission parabolas. The third shaft, from 80.50 m to 98.00 m, has a circular tubular section with an outer diameter of 3.00 m and thickness of 0.25 m; its outer surface carries four tubular steel uprights that support other parabolas.

In Table 1, the properties of the two structures are reported, including the first three fundamental frequencies, modal masses, and the damping ratio, while the first three mode shapes and the width along the height are reported in Figure 2.

3.2. Thunderstorm Wind Velocity and Loading Modeling

The data employed in the study were recorded by 14 bi- or tri-axial ultrasonic anemometers installed in the ports of Genoa, La Spezia, Livorno, and Savona by the Department of Civil, Chemical, and Environmental Engineering (DICCA), and include 129 thunderstorm outflow records at a duration of 10 min [43]. Anemometers were mounted at a height, h_a , reaching at least 10 m above the ground, mainly on high-rise towers or antenna masts at the top of buildings, in order to avoid local effects and to register undisturbed wind velocities. Figure 3 shows, as an example, one anemometer per each location considered.

Table 1. Main properties of the two structure test cases.

Structure	H [m]	n_1 [Hz]	n_2 [Hz]	n_3 [Hz]	m_1 [kg]	m_2 [kg]	m_3 [kg]	ζ
Lighting pole	15.76	0.53	3.16	8.76	164.37	83.65	46.17	0.002
Telecommunications tower	98	0.49	3.23	7.25	482,989.76	166,620.00	53,764.00	0.005

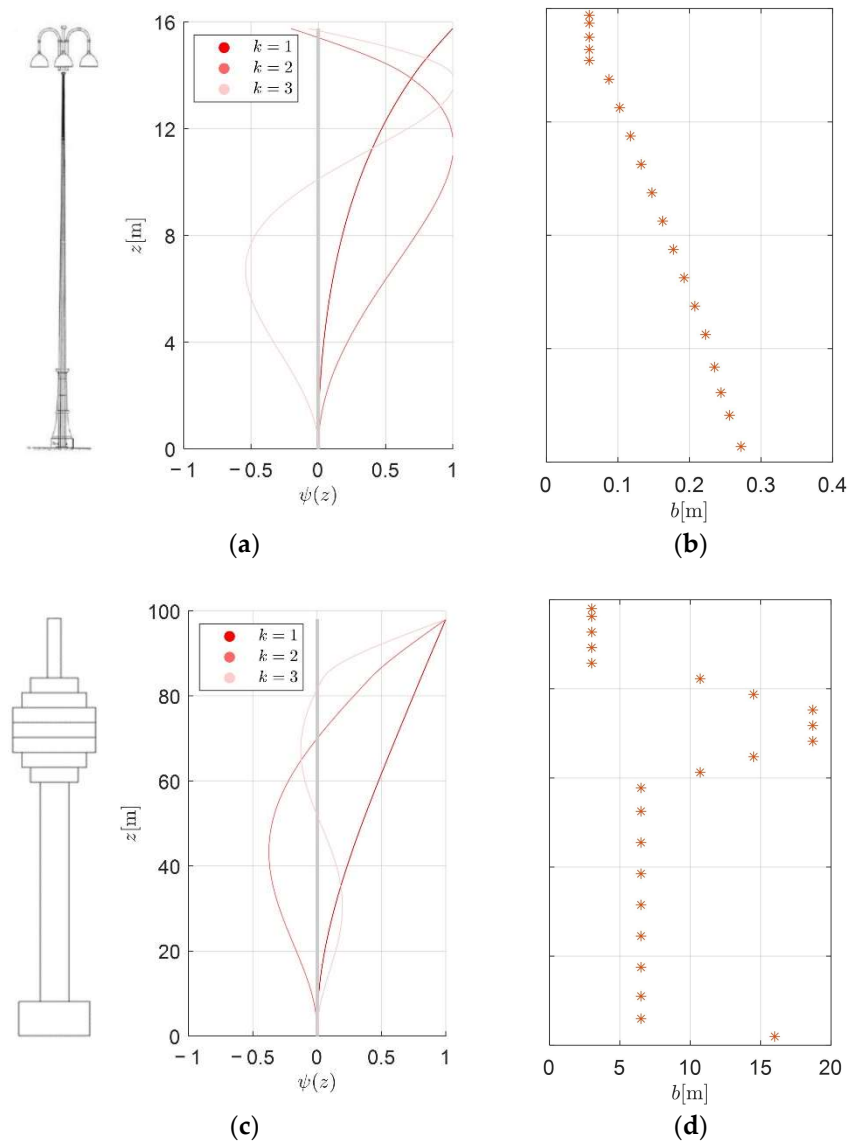


Figure 2. Vibration modes: (a) lighting pole, (c) telecommunications tower; width of the structure (star dots): (b) lighting pole, (d) telecommunications tower.



Figure 3. Cont.

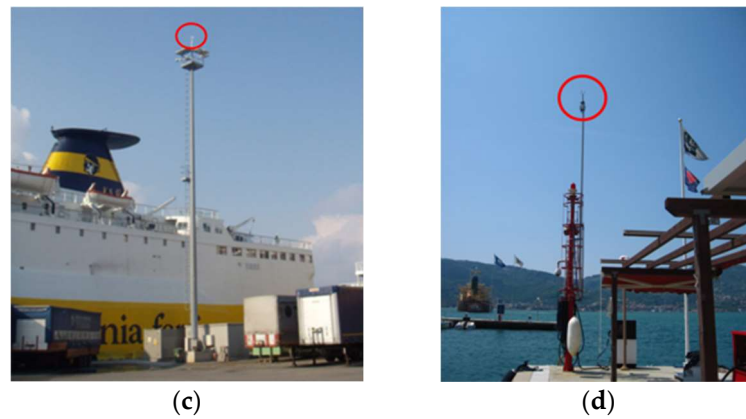


Figure 3. Anemometers in the port areas of (a) Genoa ($h_a = 61.4$ m); (b) Livorno ($h_a = 75$ m); (c) Savona ($h_a = 28$ m); and (d) La Spezia ($h_a = 10$ m).

All the anemometers have a sampling rate of 10 Hz, a precision of 0.01 m/s for the velocity, and 1° for the direction. A detailed study of the data collected has been carried out by Zhang et al. [29]. As an example, Figure 4 shows four samples of thunderstorm wind speeds recorded in the ports of Genoa, Livorno, Savona, and La Spezia.

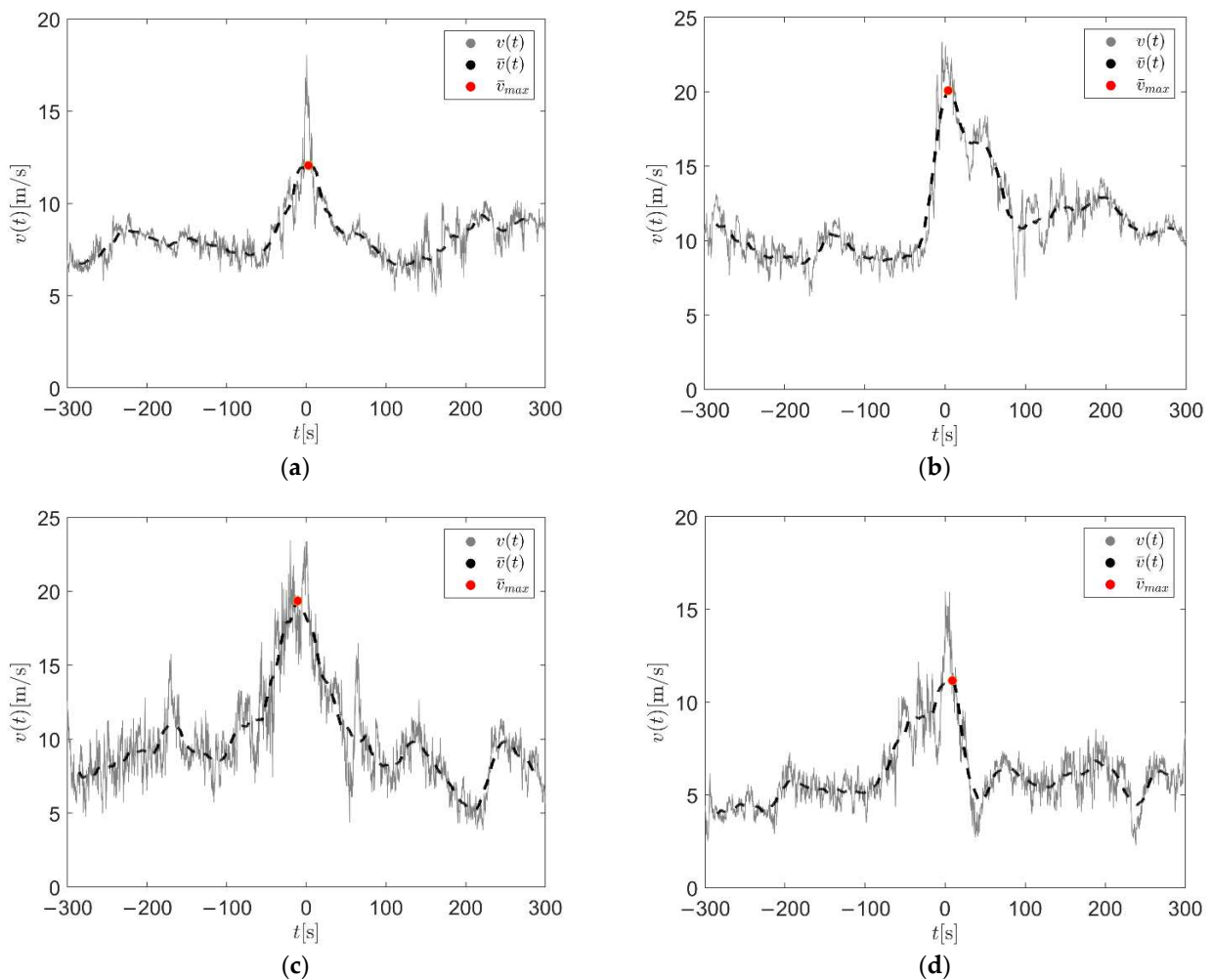


Figure 4. Examples of recorded thunderstorm wind speeds in different ports (slowly varying mean wind speed in dashed lines): (a) Genoa ($h_a = 61.4$ m); (b) Livorno ($h_a = 75$ m); (c) Savona ($h_a = 28$ m); (d) La Spezia ($h_a = 10$ m).

The ensemble values of the maximum mean wind speed, turbulence intensity, and integral length scale read $\bar{v}_{\max} = 16.01$ m/s, $\bar{I}_v = 0.12$, and $L_v = 27.32$ m, respectively [20,29], while the modulating function $\gamma(t)$ of the slowly varying mean wind speed average trend is defined according to the model of Roncallo and Tubino [38]:

$$\gamma(t) = \begin{cases} \frac{1-\gamma^*}{2} [\cos(\frac{2\pi t}{T}) + 1] + \gamma^* & , |t| < \frac{T}{2} \\ \gamma^* & , |t| \geq \frac{T}{2} \end{cases} \quad (43)$$

where the parameters $\gamma^* = 0.54$ and $T = 169.81$ s. Concerning the vertical profile of the mean wind velocity associated with the thunderstorm outflow, the model from Wood and Kwok [44] is adopted as outlined in Appendix A (Equation (A1)). The analyses are carried out by fixing $h = 20$ m and using the different values of the nose height, i.e., $z_m = 25, 50, 75, 100$ m. As an example, the vertical mean speed profile of the thunderstorm outflow and synoptic wind are plotted in Figure 5a,b for the lighting pole and telecommunications tower, respectively. Note that for the lighting pole (Figure 5a), the typical nose shape is not visible since the nose tip is located above the structure, whilst it is clearly detectable for the telecommunications tower, especially at lower values of z_m .

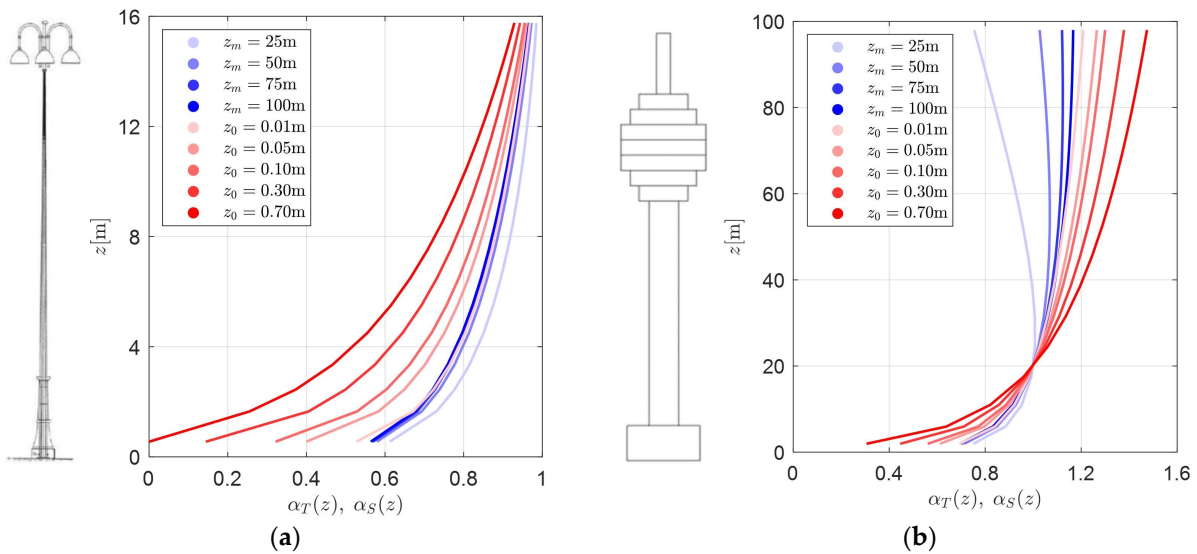


Figure 5. Vertical mean speed profile of the thunderstorm outflow (blue lines) and synoptic wind (red lines): (a) lighting pole; (b) telecommunications tower.

It is worth pointing out that the profiles also follow the model in Equation (A2) for lower values of z , whilst the guidelines suggest assuming a constant profile below a certain height, fixed according to the exposure category [40]. This recommendation is disregarded for the purpose of showing the differences between the thunderstorm and synoptic events from a theoretical point of view.

Concerning the turbulence intensity, its dependence on the height above the ground and roughness length is still a matter of discussion. Studies in the literature based on a large amount of full-scale data have shown that the dependence of the turbulence intensity on the ratio z/z_0 is weak [5,29], and the values observed are on average lower than the ones associated with synoptic winds. However, these studies were based on data collected by anemometers located in coastal areas, and thus have similar roughness lengths with which it is difficult to detect a significant dependence on the roughness. Other studies carried out on different sites have shown increasing trends for the vertical profile of the turbulence intensity, as well as greater values comparable to those observed during synoptic events [45–47]. Moreover, it was shown that the vertical profile of the turbulence intensity on the height changes during the thunderstorm, showing a decreasing trend during the ramp-up phase of the wind speed [32]. In order to carry out a meaningful comparison with

the synoptic case, two different models covering the possible scenarios of the turbulence intensity of the thunderstorm are investigated:

- a. $\theta_T(z) = 1, I_v(h) = 1/\ln\left(\frac{h}{z_0}\right)$ as the synoptic case [40];
- b. $\theta_T(z)$ provided by Equation (A3) (Appendix A), $I_v(h) = 1/\ln\left(\frac{h}{z_0}\right)$.

Figure 6 plots the vertical profiles of the turbulence intensity of the thunderstorm (Equation (A3)) and synoptic wind (Equation (A4)) events for the two structures.

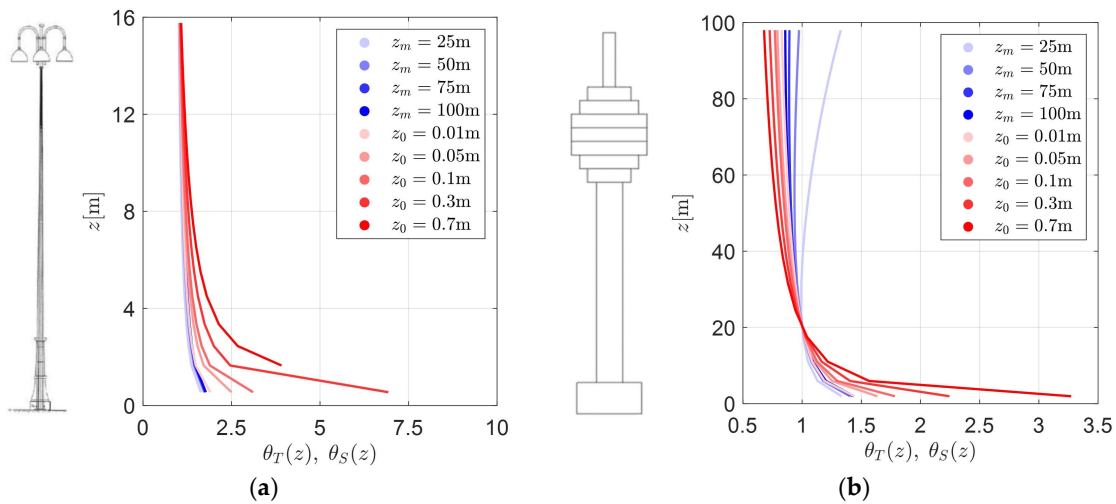


Figure 6. Vertical profile of the turbulence intensity of the thunderstorm (blue lines, Equation (A3)) and synoptic wind (red lines, Equation (A4)) events: (a) lighting pole; (b) telecommunications tower.

The definition of the mean wind loading is pursued through the derivation of the drag coefficients and the calculation of the parameter a_1 (Equation (17)). The drag coefficients of the two structures are evaluated according to the Italian CNR guidelines [40]. Due to its cross-section with sharp corners, the drag coefficient of the lighting pole does not depend on the Reynolds number and hence on the wind velocity. Moreover, the contributions of the drag due to the metallic bell at the base of the pole and the lighting devices at the top are neglected in these analyses. Instead, the telecommunications tower presents a circular cross-section, and thus the drag coefficient depends on the Reynolds number and on the vertical profile of the wind velocity. The drag coefficients for the two structures are plotted in Figure 7.

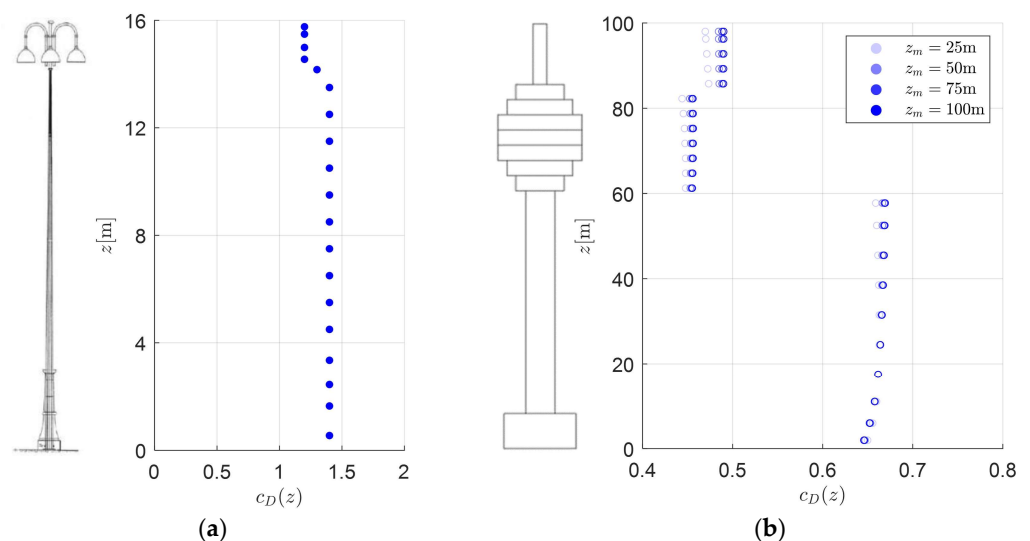


Figure 7. Drag coefficients: (a) lighting pole; (b) telecommunications tower.

It is worth pointing out that the drag coefficient adopted corresponds to a stationary wind field. Suitable aerodynamic coefficients able to account for the transient nature of thunderstorm outflows are a matter of current research; however, recent studies have shown that these effects are negligible [48,49].

3.3. Maximum Dynamic Response to Thunderstorms: Comparison among Different Approaches

In this section, the maximum dynamic response estimated with the TGRF technique (Section 2.3) is compared with the one obtained using TDA and TRS [16]. The maximum response is estimated via TDA, starting from the set of wind speed records outlined in Section 3.2. To simplify the calculations, the EWS technique by Solari [42] is employed, which consists of replacing the actual reduced turbulent fluctuation—the random function of time and space—with an equivalent turbulent fluctuation perfectly coherent in space. Assuming that the coherence function of the reduced turbulent fluctuation is expressed by Equation (6), the equivalent turbulent fluctuation is obtained following the steps reported by Solari [18] and Solari and De Gaetano [16]. Once the equivalent wind speed is determined, the wind loading and the first modal force are derived by Equations (8)–(10) and (13), and the dynamic response is calculated by integrating the equation of motion into Equation (12). Finally, the maximum dynamic response is estimated by taking the maximum value of Equation (11), considering $z = H$. Considering the TRS technique, the diagrams from Solari and De Gaetano [16] are adopted. Since [16] does not furnish values of the TRS for $\zeta = 0.005$, for the telecommunications tower, it is estimated through a linear interpolation between the values $\zeta = 0.002$ and $\zeta = 0.01$. Moreover, in order to provide a consistent comparison with the TRS, the turbulence intensity is assumed to be constant with the height—i.e., $\theta(z) = 1$ —and equal to the average value extracted from the data (Section 3.2). For the TDA, the maximum dynamic response is reported in terms of average value together with a confidence interval of one standard deviation. The comparison in terms of maximum response is reported in Figure 8 on varying the height of the nose z_m .

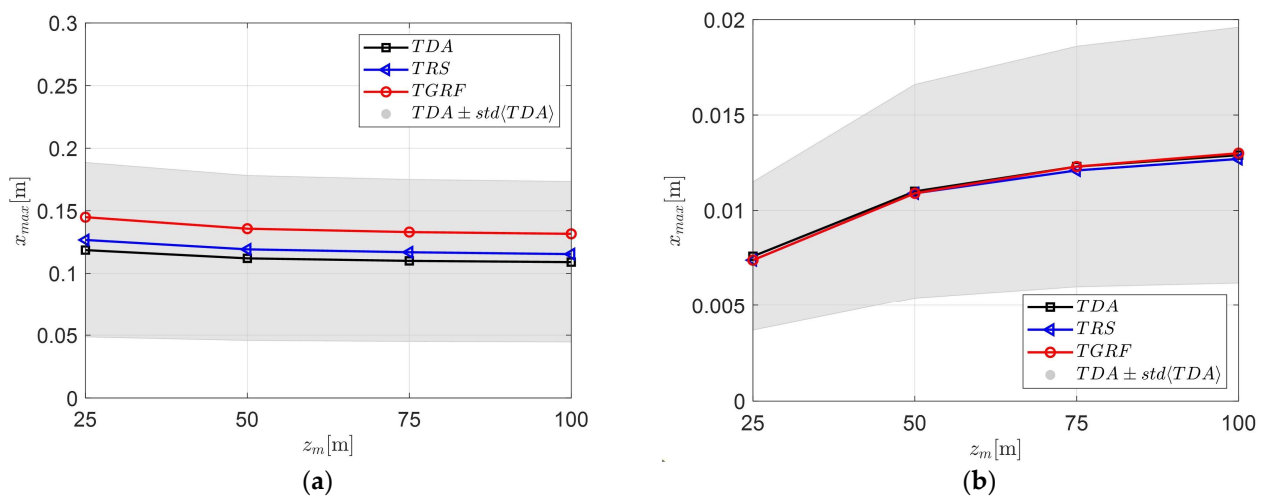


Figure 8. Maximum response evaluated with the three approaches (TDA in black lines and its value plus/minus one standard deviation in the grey area; TRS—blue lines; and TGRF—red lines): (a) lighting pole; (b) telecommunications tower.

It can be observed that the three approaches are in good agreement with each other, especially for the telecommunications tower (Figure 8b). More specifically, for the lighting pole (Figure 8a), TDA and TRS furnish very close trends, almost constant with z_m , while the TGRF furnishes slightly more conservative results which, however, lie within the confidence interval of one standard deviation obtained using TDA. Instead, the results obtained for the telecommunications tower (Figure 8b) show an almost perfect agreement. In this case, the maximum dynamic response tends to increase upon increasing z_m . The different behavior of the trends with z_m observed for the two structures is explained by

the proximity of the tip of the nose-shaped profile of the mean wind speed with their height, which produces a greater wind loading. For the lighting pole—which can be regarded as a low-rise structure—the more z_m is reduced, the more it approaches its height, and thus provides greater wind loading on the structure (Figure 7a). Conversely, for the telecommunications tower, the more z_m is increased, the more the nose tip reaches its top, providing greater wind speeds, and thus results in a greater wind loading on the structure (Figure 5b). This aspect reflects the well-known characteristic of thunderstorm outflows, i.e., the threat they provide for mid-low structures.

Overall, from the results shown in Figure 8, it can be concluded that the three methods adopted for the estimate of the maximum response are in good agreement with each other. In particular, TRS furnishes a good estimate, but its derivation may not be so straightforward due to it being based on diagrams; the TGRF may provide some overestimation for low-damped structures; however, it constitutes a reliable and handy tool for engineers in virtue of the closed-form solution provided.

4. Comparison between Thunderstorm and Synoptic Dynamic Response

In light of the considerations on the TGRF outlined in the previous sections, in this section, the method is adopted in the spirit of comparing the maximum response provided by a thunderstorm outflow and a synoptic wind following a code-based approach. The ratio between the maximum response to the thunderstorm ($x_{\max,T}$) and the synoptic event ($x_{\max,S}$) is defined as follows:

$$\frac{x_{\max,T}}{x_{\max,S}} = R_v R_a R_G \quad (44)$$

where the three quantities R_v , R_a , and R_G are the reference velocity ratio, the velocity profile ratio, and the gust response factor ratio, respectively (Equations (24) and (42)). They are defined as follows:

$$R_v = \frac{\bar{v}_{\max}^2(h)}{\bar{v}_S^2(h)} \quad (45)$$

$$R_a = \frac{a_{1,T}}{a_{1,S}} \quad (46)$$

$$R_G = \frac{G_{x,T}}{G_{x,S}} \quad (47)$$

where \bar{v}_S is the reference wind velocity associated with the synoptic wind. Using Equation (44), this follows:

$$x_{\max,T} = R_v R_a R_G x_{\max,S} \quad (48)$$

which is conceptually similar to the gust front factor framework proposed by Kwon and Kareem [24].

In the next paragraphs, three ratios are estimated for the two structures: the reference velocity ratio is first derived (Section 4.1) starting from statistical analyses based on full-scale data, and both the mean wind speed of the thunderstorm outflow and synoptic wind are fixed with the same return period; secondly (Section 4.2), the mean velocity profile ratio is estimated, introducing vertical profiles of the mean velocity for synoptic and thunderstorm winds (Equation (A1)); and finally (Section 4.3), the gust response factor ratio is evaluated according to the TGRF approach and the Italian guidelines [40] for thunderstorm and synoptic winds, respectively, accounting for the different modeling of the turbulence intensity (Section 3.2). The maximum response is thus derived and compared according to Equation (48) (Section 4.4).

4.1. Reference Velocity Ratio R_v

The wind speed is defined following the spirit of design codes and standards. In this example, the Italian Guide for the Assessment of Wind Actions and Effects on Structures [40] is taken as a reference. The mean wind speed for thunderstorm outflow and for synoptic events with a mean return period of 50 years are derived from statistical analyses carried out by Zhang et al. [10] on full-scale anemometer data. In particular, the wind velocity collected from an anemometer in the port of Livorno in the High Tyrrhenian Sea is considered, located at 20 m above the ground. Table 2 summarizes the main properties of the wind velocity data of both the thunderstorm outflow (T) and synoptic event (S) that are employed in this study. The mean wind speeds with a return period of 50 years are obtained from the peak wind velocities $\hat{v}_{\max}(h)$ and $\hat{v}_S(h)$ as $\bar{v}_{\max}(h) = \hat{v}_{\max}(h)/G_{v,T}$ and $\bar{v}_S(h) = \hat{v}_S(h)/G_{v,S}$, respectively, where $G_{v,T}$ and $G_{v,S}$ are the gust factor of the thunderstorm and synoptic wind velocities, respectively [10].

Table 2. Main wind velocity parameters.

h [m]	$\hat{v}_{\max}(h)$ [m/s]	$\hat{v}_S(h)$ [m/s]	$G_{v,T}$	$G_{v,S}$	$\bar{v}_{\max}(h)$ [m/s]	$\bar{v}_S(h)$ [m/s]	R_v
20	38.33	33.85	1.140	1.471	33.62	23.01	2.135

It can be noticed that the mean wind velocity in Table 2 associated with synoptic winds $\bar{v}_S(h)$ is significantly lower than the reference value of 28 m/s furnished in [40], which is associated with a reference height $h = 10$ m, a return period of 50 years, and flat terrain with $z_0 = 0.05$ m. This is due to the fact that the values reported in codes are based on statistical analyses that do not distinguish between wind events of a different nature, and hence they provide intermediate values between velocities associated with thunderstorms and synoptic winds [10,50]. In this framework, the data in Table 2 furnish a more authentic value for synoptic winds being the result of an accurate separation procedure [51]. Moreover, it is important to observe that the maximum mean wind speed due to thunderstorms is greater than the one related to synoptic events by 46%, which leads to a value of the reference velocity ratio R_v of greater than two. It is worth pointing out that since the reference velocity depends on the reference height according to the vertical profile of the mean wind speed, the reference velocity ratio R_v also depends on the reference height. For low reference heights, where the thunderstorm profile is generally larger than the synoptic one, $R_v > 1$ is expected. Finally, it is worth noticing that the analyses are based on the data collected in a thunderstorm-prone area; therefore, different statistics might be expected in other areas less affected by such extreme events.

4.2. Velocity Profile Ratio R_d

The calculation of parameter a_1 (Equation (17)) is pursued based on the vertical profiles of the mean wind speed, as outlined in Appendix A (Equation (A2)), and by defining the drag coefficients of the two structures according to [40]. Analyses are carried out for different values of the roughness length $z_0 = 0.01, 0.05, 0.10, 0.30, 0.70$ m. It is worth pointing out that, with the aim of inspecting different varying wind profiles z_0 , the wind velocities in Table 2 should be scaled, in principle, according to the fixed roughness length. However, since there is no established relation between \bar{v}_{\max} and z_0 for thunderstorms, in order to secure consistency between the thunderstorm and synoptic wind velocities recorded by the same anemometer, this scaling is disregarded. Hence, the effects of the roughness length are only accounted for in the definition of the shape of the vertical profile according to Equation (A2), while for the thunderstorm outflow, different shapes are investigated by varying the nose tip through parameter z_m according to Equation (A1). The drag coefficients due to the synoptic wind for the telecommunications tower are reported in Figure 9.

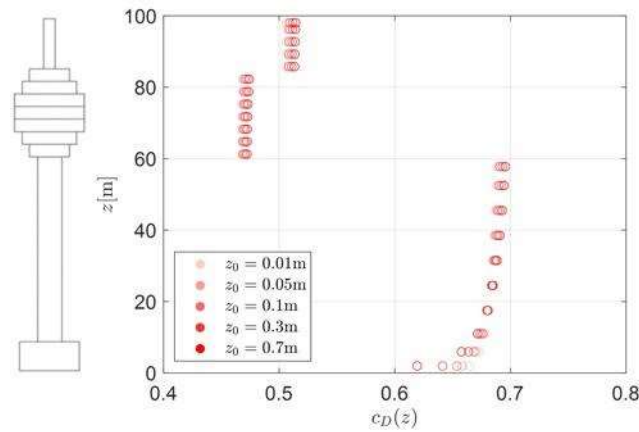


Figure 9. Drag coefficient of the telecommunications tower associated with the synoptic wind.

Figure 10 plots the velocity profile ratio on varying z_m and z_0 , for the lighting pole (Figure 10a) and the telecommunications tower (Figure 10b), respectively.

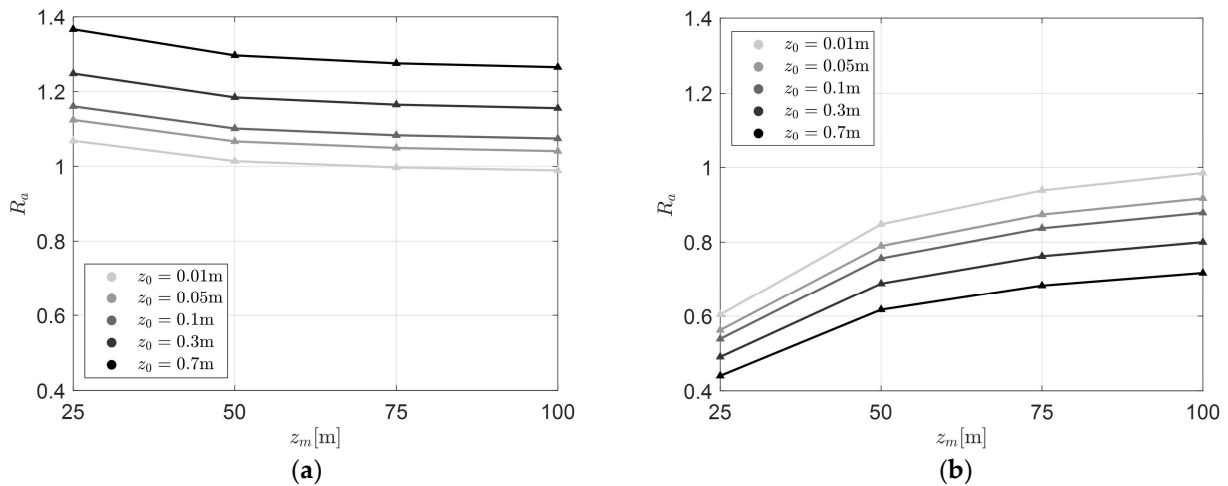


Figure 10. Velocity profile ratio R_a evaluated for the thunderstorm and synoptic event: (a) lighting pole; (b) telecommunications tower.

Figure 10a shows that for the lighting pole, R_a is always higher than unity, except for the low roughness length ($z_0 = 0.01$ m) and high nose tip ($z_m = 75$ m and $z_m = 100$ m), showing an increasing trend with z_0 while decreasing with z_m . Conversely, for the telecommunications tower (Figure 10b), the trends are opposite. Indeed, it can be noticed that R_a is always lower than unity, and it reduces upon increasing z_0 , while it increases upon increasing z_m . The different behaviors observed for the two structures with z_m are due to the different positions of the tip of the nose with respect to the reference height, and therefore the different shapes of the vertical mean wind profiles. It can be argued that the thunderstorm provides a greater wind loading for the pole and a smaller one for the tower compared with the wind loading provided by the synoptic case.

Overall, the results are in accordance with the wind velocity profiles reported in Figure 5, and emphasize the greater sensitivity of low-rise structures (such as the lighting pole) to thunderstorm outflows.

4.3. Gust Response Factor Ratio R_G

The gust factor of the response is derived according to Section 2.3 following the two different approaches for the turbulence intensity outlined in Section 3.2. The integral length scale is instead estimated as for the synoptic case (Appendix A, Equation (A5)).

Figure 11 plots the gust response factor ratio for the lighting pole (Figure 11a) and the telecommunications tower (Figure 11b), evaluated according to the two different models of the turbulence intensity; i.e., case (a) $\theta_T(z) = 1$ varying the roughness length (Section 3.2) and case (b) assuming the vertical profile in Equation (A3) (Appendix A).

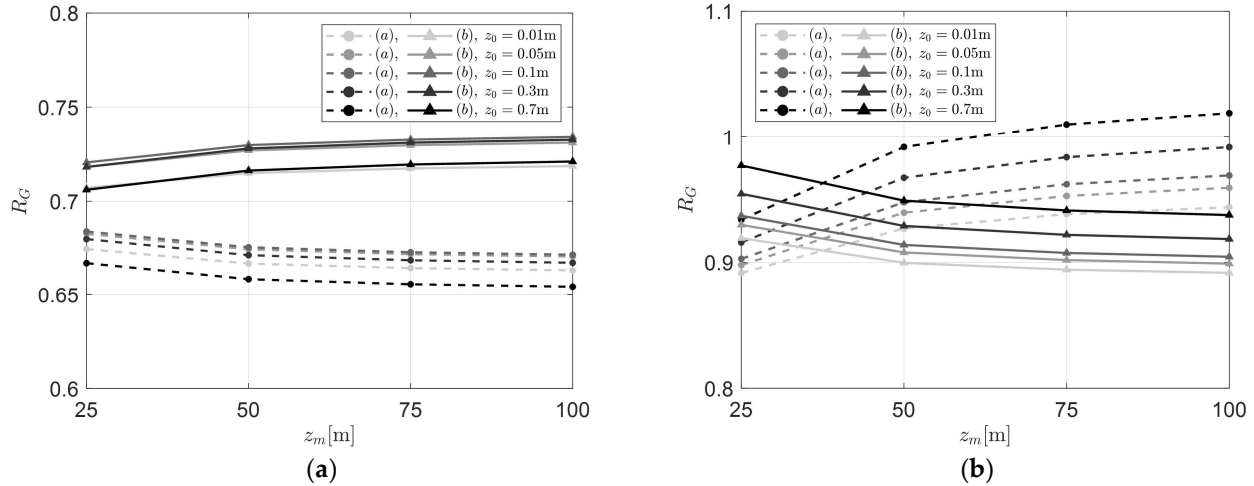


Figure 11. Gust response factor ratio R_G . Case (a) circles—dashed lines; case (b) triangles—solid lines; lighting pole (a); and telecommunications tower (b).

Figure 11 shows that when moving from case (a) to case (b), R_G tends to increase for the low-rise structure (Figure 9a), while a reduction is observed for the taller one (Figure 9b), except for low values of z_m . In this latter case, the dependence on z_0 is more marked because of the greater height of the structure. Moreover, the pole R_G in case (a) tends to decrease with z_m (Figure 11a), while it increases upon increasing z_m in case (b) (solid lines). The opposite behavior is instead observed for the tower (Figure 9b).

It is important to notice that for both structures, the gust response ratio is always lower than unity. This is due to the transient dynamic effects induced by the nonstationary loading of the thunderstorm that mitigates the response [13]. The only exception is observed for the tower when the turbulence intensity of the thunderstorm is assumed to be constant with the height, but variable with the roughness length for higher values of z_0 and z_m . This is due to the combination of a lower turbulence intensity of the synoptic wind (estimated at the equivalent height), and a larger value of the resonance factor (Equation (26)) as a result of a larger vertical mean speed profile.

Finally, it can be observed that for the lighting pole—i.e., the low-rise structure—the gust response factor results are weakly dependent on both the roughness length and the height of the nose of the vertical profile. Therefore, future studies may investigate whether this behavior occurs after introducing a relation between z_0 and z_m in the modeling of the vertical profile.

4.4. Maximum Response

The comparison between the maximum dynamic responses is performed according to Equation (44). It can be observed that among the three quantities in Equations (45)–(47), R_v is clearly the greater one, being $\bar{v}_{\max}^2(h) \gg \bar{v}_S^2(h)$ (Table 2). This quantity is independent of z_0 and z_m , and scales the product among the other two ratios.

Figure 12 plots the ratios between the maximum response to the thunderstorm and the synoptic wind for both the lighting pole (Figure 12a) and the telecommunications tower (Figure 12b), which are estimated according to the two models of the thunderstorm turbulence intensity (Section 3.2).

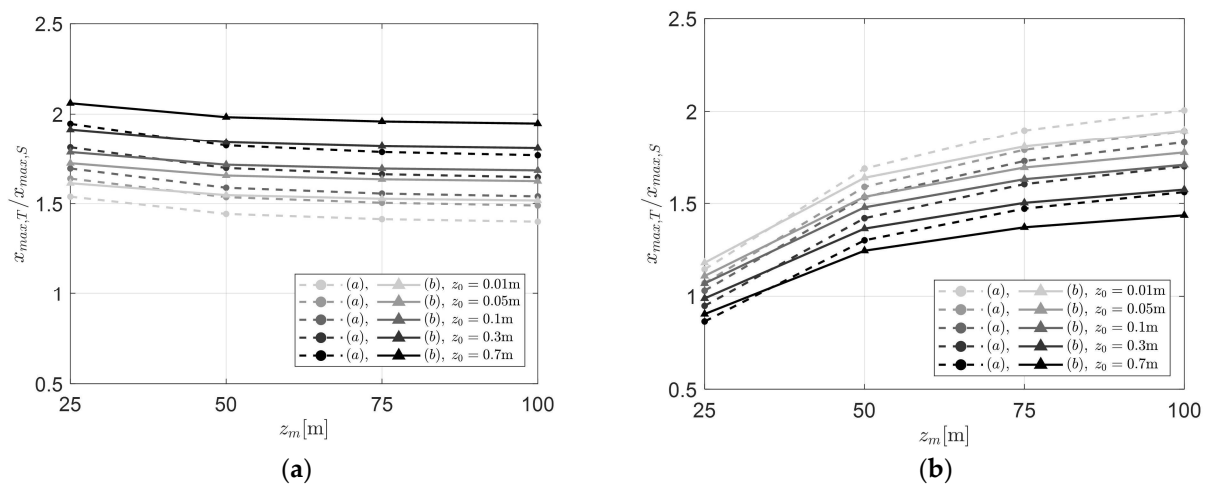


Figure 12. Maximum response ratios. Case (a) circles—dashed lines; case (b) triangles—solid lines; lighting pole (a); and telecommunications tower (b).

Figure 12 shows that for the pole, the ratio between the maximum responses has a weak dependence on z_m , while the dependence on z_0 is more marked for the tower (Figure 12b). Nevertheless, the dependence on the roughness length is not negligible, leading to an increase in the maximum response due to the thunderstorm for the pole and a decrease for the tower. It is also observed that moving from the hypothesis of constant turbulence intensity (case a, dashed lines) to account for its variability with the height (case b, solid lines), the ratio between the maximum response due to the thunderstorm and the synoptic wind of the pole increases, especially for higher values of z_0 and z_m (Figure 12a), whilst for the tower a reduction is observed, especially for larger values of z_m (Figure 12b). These results point out that the impact of the model of the turbulence intensity vertical profile may not be negligible in the estimate of the maximum dynamic response due to the thunderstorm, especially for a low-rise structure where neglecting the dependence on the height may not be conservative. Nevertheless, the dependence of the turbulence intensity on the roughness length of the site seems to play an important role that is not negligible in determining an accurate estimate of the maximum response and wind loading. Finally, it can be observed that for both structures, the thunderstorm provides a larger maximum response compared with the synoptic wind, reaching twice the maximum response given by the latter when the height of the nose-shaped profile is close to the tip of the structure. Higher responses due to the synoptic wind are observed for the tower for lower values of z_m (Figure 12b), where the tip of the nose profile affects the structure only in its lowest part. Finally, it should be stressed that the obtained results are strongly affected by the reference velocity ratio R_v . In this study, the value considered was derived from data collected in thunderstorm-prone areas, leading to a factor greater than two. However, in case the two reference wind speeds are similar, the velocity ratio tends to unity, and the curves in Figure 12 drop below one. As a result, if R_v is close to unity, the synoptic wind provides the greatest dynamic response. In light of this consideration, it would be important to define a criterion to establish whether a site is thunderstorm-prone or not, similar to the earthquake case. Finally, it is interesting to investigate whether these results hold when a vertical nose-shaped profile that accounts for the roughness length is considered.

5. Conclusions and Prospects

In this study, the thunderstorm gust response factor was generalized to the analysis of slender vertical structures, and it was employed for a comparison between the maximum dynamic response due to thunderstorms and synoptic events. Two real structures were considered as case studies; i.e., a lighting pole, regarded as a low-rise structure, and a telecommunications tower, regarded as a higher structure. The comparison between the maximum dynamic response due to thunderstorms and synoptic events was carried

out by investigating the role of the roughness length, the height of the nose profile, and turbulence intensity.

From the comparison with TDA and TRS, it can be concluded that the TGRF was proven to be a robust and reliable tool for the estimate of the maximum response of slender vertical structures.

In view of the results outlined, the TGRF was then adopted to carry out a comparison with stationary wind.

The comparison showed that both the definition of the reference wind speed and the height of the nose tip of the thunderstorm mean wind profile are crucial for the maximum response. According to the available data collected in a thunderstorm-prone area for a return period of 50 years, it was pointed out how the velocity ratio is significantly large, and that the thunderstorm provides the design loading condition in most of the cases except for the taller structure, where the synoptic wind provides the design conditions only if the nose tip is at the lowest height. In this framework, it was shown that accounting for the transient dynamics in the estimate of the gust response factor is beneficial for the reduction in the maximum response due to thunderstorms. Moreover, the dependence on the roughness length is crucial for a proper estimate of the maximum response and wind loading.

The results shed light on some important aspects that need to be addressed. Firstly, the importance of carrying out an accurate estimate of the reference wind speed through separated statistical analyses of thunderstorms and synoptic events was highlighted, especially in thunderstorm-prone areas. Secondly, further studies are necessary for the definition of suitable analytical models that are able to account for the dependence of the vertical mean wind speed profile and turbulence intensity on the roughness length.

In view of these results, the evaluation of the wind loading due to thunderstorm outflows is essential for a safer and cost-efficient design of structures, and the introduction of proper guidelines in codes and standards is advisable. In this framework, the TGRF approach represents a robust and handy tool for engineers to properly estimate the maximum response and wind loading caused via thunderstorms.

Future studies will be aimed at carrying out a comparison between the maximum dynamic response registered from a monitored slender structure and the one estimated through the TGRF technique.

Author Contributions: Conceptualization, L.R. and F.T.; methodology, L.R. and F.T.; software (Matlab 2020), L.R. and M.G.; validation, L.R. and M.G.; formal analysis, L.R. and M.G.; investigation, L.R.; resources, L.R. and F.T.; data curation, L.R. and M.G.; writing—original draft preparation, L.R.; writing—review and editing, F.T.; visualization, L.R. and M.G.; supervision, F.T. All authors have read and agreed to the published version of the manuscript.

Funding: This research was funded by the European Research Council (ERC) under the European Union's Horizon 2020 Research and Innovation Program (grant agreement No.: 741273) for the project THUNDERR—Detection, simulation, modelling, and loading of thunderstorm outflows to design wind-safe and cost-efficient structures—supported by an Advanced Grant 2016. The data used for this research were recorded via the monitoring network set up as part of the European Projects Winds and Ports (grant No.: B87E09000000007) and Wind, Ports, and Sea (grant No.: B82F13000100005), funded by the European Territorial Cooperation Objective, Cross-border Program Italy–France Maritime 2007–2013.

Institutional Review Board Statement: Not applicable.

Informed Consent Statement: Not applicable.

Data Availability Statement: Data are available upon reasonable request from the corresponding author.

Acknowledgments: The authors are grateful to Giovanni Solari who inspired, motivated, and oversaw this research.

Conflicts of Interest: The authors declare no conflict of interest.

Appendix A Vertical Profiles of the Mean Wind Speed, Turbulence Intensity, and Integral Length Scale

In this appendix, the models of the vertical profiles of the mean wind speed and turbulence intensity of both the thunderstorm outflow and synoptic wind are illustrated.

The vertical profile of the mean wind speed of the thunderstorm outflow is modeled according to the expression provided by Wood and Kwok [44]. Thus, the function $\alpha(z)$ is given by [18]:

$$\alpha(z) = \alpha_T(z) = \left(\frac{z}{h}\right)^{1/6} \frac{1 - \operatorname{erf}\left(0.70 \frac{z}{z^*}\right)}{1 - \operatorname{erf}\left(0.70 \frac{h}{z^*}\right)} \quad (\text{A1})$$

where $\operatorname{erf}(z)$ is the error function, $z^* = 6z_m$ is the height for which $\bar{v}_{\max}(z^*) = 0.5\bar{v}_m$, where \bar{v}_m is the maximum value of \bar{v}_{\max} along z , z_m is the height for which $\bar{v}_{\max} = \bar{v}_m$, and h is the reference height for which $\alpha(h) = 1$.

The mean wind velocity vertical profile for synoptic winds is defined according to the logarithmic law [40]:

$$\alpha(z) = \alpha_S(z) = \frac{\ln\left(\frac{z}{z_0}\right)}{\ln\left(\frac{h}{z_0}\right)} \quad (\text{A2})$$

where z_0 is the roughness length and $\alpha_S(h) = 1$. It is worth noticing that the nose-shaped profile in Equation (A1) does not depend on the roughness length of the logarithmic one in Equation (A2), and it is instead governed only by the parameter z_m .

With the aim of introducing a tentative model for the vertical profile of the thunderstorm turbulence intensity in analogy with the synoptic case, the inverse of the mean wind speed profile is chosen, and it reads:

$$\theta(z) = \theta_T(z) = \frac{1 - \operatorname{erf}\left(0.70 \frac{h}{z^*}\right)}{\left(\frac{z}{h}\right)^{1/6} [1 - \operatorname{erf}\left(0.70 \frac{z}{z^*}\right)]} \quad (\text{A3})$$

It is worth noticing that Equation (A3) implicitly assumes that the standard deviation of the turbulence does not change with the height.

The turbulence intensity profile for the synoptic wind is modeled according to the relation provided in [40]:

$$\theta(z) = \theta_S(z) = \frac{\ln\left(\frac{h}{z_0}\right)}{\ln\left(\frac{z}{z_0}\right)} \quad (\text{A4})$$

The integral length scale is estimated as follows [40,52]:

$$L_v(z) = \bar{L} \left(\frac{z}{\bar{z}}\right)^v \quad (\text{A5})$$

where $v = 0.67 + 0.05 \ln(z_0)$, $\bar{L} = 300$ m, and $\bar{z} = 200$ m.

References

1. Repetto, M.P.; Solari, G. Equivalent Static Wind Actions on Vertical Structures. *J. Wind Eng. Ind. Aerodyn.* **2004**, *92*, 335–357. [\[CrossRef\]](#)
2. Repetto, M.P.; Solari, G. Wind-Induced Fatigue Collapse of Real Slender Structures. *Eng. Struct.* **2010**, *32*, 3888–3898. [\[CrossRef\]](#)
3. Fujita, T. Downbursts: Meteorological Features and Wind Field Characteristics. *J. Wind Eng. Ind. Aerodyn.* **1990**, *36*, 75–86. [\[CrossRef\]](#)
4. Sengupta, A.; Sarkar, P.P. Experimental Measurement and Numerical Simulation of an Impinging Jet with Application to Thunderstorm Microburst Winds. *J. Wind Eng. Ind. Aerodyn.* **2008**, *96*, 345–365. [\[CrossRef\]](#)
5. Solari, G.; Burlando, M.; De Gaetano, P.; Repetto, M.P. Characteristics of Thunderstorms Relevant to the Wind Loading of Structures. *Wind. Struct. Int. J.* **2015**, *20*, 763–791. [\[CrossRef\]](#)
6. Lombardo, F.T.; Smith, D.A.; Schroeder, J.L.; Mehta, K.C. Thunderstorm Characteristics of Importance to Wind Engineering. *J. Wind Eng. Ind. Aerodyn.* **2014**, *125*, 121–132. [\[CrossRef\]](#)

7. Harris, R.I. The Level Crossing Method Applied to Mean Wind Speeds from “Mixed” Climates. *Struct. Saf.* **2017**, *67*, 54–61. [[CrossRef](#)]
8. Ponte, J.; Riera, J.D. Simulation of Extreme Wind Series Caused by Thunderstorms in Temperate Latitudes. *Struct. Saf.* **2010**, *32*, 231–237. [[CrossRef](#)]
9. Solari, G. Emerging Issues and New Scenarios for Wind Loading on Structures. *Wind Struct.* **2014**, *19*, 295–320. [[CrossRef](#)]
10. Zhang, S.; Solari, G.; Yang, Q.; Repetto, M.P. Extreme Wind Speed Distribution in a Mixed Wind Climate. *J. Wind Eng. Ind. Aerodyn.* **2018**, *176*, 239–253. [[CrossRef](#)]
11. Letchford, C.W.; Mans, C.; Chay, M. Thunderstorms—Their Importance in Wind Engineering (a Case for the next Generation Wind Tunnel). *J. Wind Eng. Ind. Aerodyn.* **2002**, *90*, 1415–1433. [[CrossRef](#)]
12. Fu, X.; Li, H.-N.; Li, G. Fragility Analysis and Estimation of Collapse Status for Transmission Tower Subjected to Wind and Rain Loads. *Struct. Saf.* **2016**, *58*, 1–10. [[CrossRef](#)]
13. Roncallo, L.; Solari, G.; Muscolino, G.; Tubino, F. Maximum Dynamic Response of Linear Elastic SDOF Systems Based on an Evolutionary Spectral Model for Thunderstorm Outflows. *J. Wind Eng. Ind. Aerodyn.* **2022**, *224*, 104978. [[CrossRef](#)]
14. Chen, L.; Letchford, C.W. Parametric Study on the Along-Wind Response of the CAARC Building to Downbursts in the Time Domain. *J. Wind Eng. Ind. Aerodyn.* **2004**, *92*, 703–724. [[CrossRef](#)]
15. Solari, G.; Rainisio, D.; De Gaetano, P. Hybrid Simulation of Thunderstorm Outflows and Wind-Excited Response of Structures. *Meccanica* **2017**, *52*, 3197–3220. [[CrossRef](#)]
16. Solari, G.; De Gaetano, P. Dynamic Response of Structures to Thunderstorm Outflows: Response Spectrum Technique vs Time-Domain Analysis. *Eng. Struct.* **2018**, *176*, 188–207. [[CrossRef](#)]
17. Solari, G.; De Gaetano, P.; Repetto, M.P. Thunderstorm Response Spectrum: Fundamentals and Case Study. *J. Wind Eng. Ind. Aerodyn.* **2015**, *143*, 62–77. [[CrossRef](#)]
18. Solari, G. Thunderstorm Response Spectrum Technique: Theory and Applications. *Eng. Struct.* **2016**, *108*, 28–46. [[CrossRef](#)]
19. Housner, G.W.; Martel, R.R.; Alford, J.L. Spectrum Analysis of Strong-Motion Earthquakes. *Bull. Seismol. Soc. Am.* **1953**, *43*, 97–119. [[CrossRef](#)]
20. Roncallo, L.; Solari, G. An Evolutionary Power Spectral Density Model of Thunderstorm Outflows Consistent with Real-Scale Time-History Records. *J. Wind Eng. Ind. Aerodyn.* **2020**, *203*, 104204. [[CrossRef](#)]
21. Kareem, A.; Hu, L.; Guo, Y.; Kwon, D.-K. Generalized Wind Loading Chain: Time-Frequency Modeling Framework for Nonstationary Wind Effects on Structures. *J. Struct. Eng.* **2019**, *145*, 04019092. [[CrossRef](#)]
22. Davenport, A.G. Gust Loading Factors. *J. Struct. Div.* **1967**, *93*, 11–34. [[CrossRef](#)]
23. Kwon, D.K.; Kareem, A. Gust-Front Factor: A New Framework for Wind Load Effects on Structures. *J. Struct. Eng.* **2009**, *135*, 717–732. [[CrossRef](#)]
24. Kwon, D.K.; Kareem, A. Towards Codification of Thunderstorm/Downburst Using Gust Front Factor: Model-Based and Data-Driven Perspectives. *Eng. Struct.* **2019**, *199*, 109608. [[CrossRef](#)]
25. Roncallo, L.; Tubino, F. Thunderstorm Gust Response Factor: A Closed-Form Solution. *J. Wind Eng. Ind. Aerodyn.* **2023**, *240*, 105487. [[CrossRef](#)]
26. Chen, L.; Letchford, C.W. A Deterministic-Stochastic Hybrid Model of Downbursts and Its Impact on a Cantilevered Structure. *Eng. Struct.* **2004**, *26*, 619–629. [[CrossRef](#)]
27. Chen, L.; Letchford, C.W. Numerical Simulation of Extreme Winds from Thunderstorm Downbursts. *J. Wind Eng. Ind. Aerodyn.* **2007**, *95*, 977–990. [[CrossRef](#)]
28. Choi, E.C.C.; Hidayat, F.A. Dynamic Response of Structures to Thunderstorm Winds. *Prog. Struct. Eng. Mater.* **2002**, *4*, 408–416. [[CrossRef](#)]
29. Zhang, S.; Solari, G.; De Gaetano, P.; Burlando, M.; Repetto, M.P. A Refined Analysis of Thunderstorm Outflow Characteristics Relevant to the Wind Loading of Structures. *Probabilistic Eng. Mech.* **2018**, *54*, 9–24. [[CrossRef](#)]
30. Le, V.; Caracoglia, L. Computationally Efficient Stochastic Approach for the Fragility Analysis of Vertical Structures Subjected to Thunderstorm Downburst Winds. *Eng. Struct.* **2018**, *165*, 152–169. [[CrossRef](#)]
31. Chay, M.T.; Albermani, F.; Wilson, R. Numerical and Analytical Simulation of Downburst Wind Loads. *Eng. Struct.* **2006**, *28*, 240–254. [[CrossRef](#)]
32. Canepa, F.; Burlando, M.; Solari, G. Vertical Profile Characteristics of Thunderstorm Outflows. *J. Wind Eng. Ind. Aerodyn.* **2020**, *206*, 104332. [[CrossRef](#)]
33. Burlando, M.; De Cio, A.; Pizzo, M.; Solari, G. Analysis of Wind Vertical Profiles of Thunderstorm Events in the Mediterranean. In Proceedings of the 9th Asia-Pacific Conference on Wind Engineering, Auckland, New Zealand, 3–7 December 2017; pp. 9–12.
34. Caracoglia, L. Unified Stochastic Dynamic and Damage Cost Model for the Structural Analysis of Tall Buildings in Thunderstorm-Like Winds. *ASCE-ASME J. Risk Uncertain. Eng. Syst. Part A Civ. Eng.* **2018**, *4*, 4018043. [[CrossRef](#)]
35. Aboshosha, H.; Bitsuamlak, G.; El Damatty, A. Turbulence Characterization of Downbursts Using LES. *J. Wind Eng. Ind. Aerodyn.* **2015**, *136*, 44–61. [[CrossRef](#)]
36. Peng, L.; Huang, G.; Chen, X.; Yang, Q. Evolutionary Spectra-Based Time-Varying Coherence Function and Application in Structural Response Analysis to Downburst Winds. *J. Struct. Eng.* **2018**, *144*, 04018078. [[CrossRef](#)]
37. Lin, Y.K.; Cai, G.Q. *Probabilistic Structural Dynamics: Advanced Theory and Applications*; McGraw-Hill: New York, NY, USA, 1995; ISBN 0-07-038038-4.

38. Roncallo, L.; Tubino, F. Thunderstorm Gust Response Factor: General Tendencies and Sensitivity Analysis. *J. Wind Eng. Ind. Aerodyn.* **2023**, *236*, 105376. [[CrossRef](#)]
39. Davenport, A.G. Note on the Distribution of the Largest Value of a Random Function With Application To Gust Loading. *Proc. Inst. Civ. Eng.* **1964**, *28*, 187–196. [[CrossRef](#)]
40. CNR-DT 214/2018; CNR Guide for the Assessment of Wind Actions and Effects on Structures. CONSIGLIO NAZIONALE DELLE RICERCHE (National Research Council): Rome, Italy, 2018.
41. Solari, G. Gust Buffeting.2. Dynamic Alongwind Response. *J. Struct. Eng.* **1993**, *119*, 383–398. [[CrossRef](#)]
42. Solari, G. Equivalent Wind Spectrum Technique: Theory and Applications. *J. Struct. Eng.* **1988**, *114*, 1303–1323. [[CrossRef](#)]
43. Canepa, F.; Burlando, M.; Repetto, M.P. Thunderstorm Outflows in the Mediterranean Sea Area. *Dataset* **2023**. [[CrossRef](#)]
44. Wood, G.S.; Kwok, K.C.S. *An Empirically Derived Estimate for the Mean Velocity Profile of a Thunderstorm Downburst*, 7th ed.; Australian Wind Engineering Society Workshop: Auckland, Australia, 1998.
45. Romanic, D. Mean Flow and Turbulence Characteristics of a Nocturnal Downburst Recorded on a 213-m Tall Meteorological Tower. *J. Atmos. Sci.* **2021**, *78*, 3629–3650. [[CrossRef](#)]
46. Choi, E.C.C. Wind Characteristics of Tropical Thunderstorms. *J. Wind Eng. Ind. Aerodyn.* **2000**, *84*, 215–226. [[CrossRef](#)]
47. Aldereguía Sánchez, C.; Tubino, F.; Bagnara, A.; Piccardo, G. Experimental Simulation of Thunderstorm Profiles in an Atmospheric Boundary Layer Wind Tunnel. *Appl. Sci.* **2023**, *13*, 8064. [[CrossRef](#)]
48. Mason, M.S.; Yanga, T.; George, T.; Paxton, O.; Wong, E. An Experimental Investigation of the Unsteady Pressures on Square Cylinders in a Non-Stationary Wind Field. In Proceedings of the 8th International Colloquium. on Bluff-Body Aerodynamics and Applications, Boston, MA, USA, 7–11 June 2016.
49. Yang, T.; Mason, M.S. Aerodynamic Characteristics of Rectangular Cylinders in Steady and Accelerating Wind Flow. *J. Fluids Struct.* **2019**, *90*, 246–262. [[CrossRef](#)]
50. Solari, G.; Burlando, M.; Repetto, M.P. Detection, Simulation, Modelling and Loading of Thunderstorm Outflows to Design Wind-Safer and Cost-Efficient Structures. *J. Wind Eng. Ind. Aerodyn.* **2020**, *200*, 104142. [[CrossRef](#)]
51. De Gaetano, P.; Repetto, M.P.; Repetto, T.; Solari, G. Separation and Classification of Extreme Wind Events from Anemometric Records. *J. Wind Eng. Ind. Aerodyn.* **2014**, *126*, 132–143. [[CrossRef](#)]
52. Solari, G.; Piccardo, G. Probabilistic 3-D Turbulence Modeling for Gust Buffeting of Structures. *Probabilistic Eng. Mech.* **2001**, *16*, 73–86. [[CrossRef](#)]

Disclaimer/Publisher’s Note: The statements, opinions and data contained in all publications are solely those of the individual author(s) and contributor(s) and not of MDPI and/or the editor(s). MDPI and/or the editor(s) disclaim responsibility for any injury to people or property resulting from any ideas, methods, instructions or products referred to in the content.